Acoustic dipole and monopole effects in solid particle interaction dynamics during acoustophoresis

Davood Saeidi, Mohsen Saghafian, Shaghayegh Haghjooy Javanmard, Björn Hammarström, and Martin Wiklund

Citation: The Journal of the Acoustical Society of America **145**, 3311 (2019); doi: 10.1121/1.5110303
View online: https://doi.org/10.1121/1.5110303
View Table of Contents: https://asa.scitation.org/toc/jas/145/6
Published by the Acoustical Society of America

Acoustic dipole and monopole effects in solid particle interaction dynamics during acoustophoresis

Davood Saeidi,[1,a)] Mohsen Saghafian,[1] Shaghayegh Haghjooy Javanmard,[2] Björn Hammarström,[3] and Martin Wiklund[3,b)]
[1]*Department of Mechanical Engineering, Isfahan University of Technology, Isfahan, Iran*
[2]*Applied Physiology Research Center, Cardiovascular Research Institute, Department of Physiology, Isfahan University of Medical Sciences, Isfahan, Iran*
[3]*Department of Applied Physics, Royal Institute of Technology, KTH-AlbaNova, Stockholm, Sweden*

(Received 4 December 2018; revised 1 May 2019; accepted 15 May 2019; published online 6 June 2019)

A method is presented for measurements of secondary acoustic radiation forces acting on solid particles in a plain ultrasonic standing wave. The method allows for measurements of acoustic interaction forces between particles located in arbitrary positions such as in between a pressure node and a pressure antinode. By utilizing a model that considers both density- and compressibility-dependent effects, the observed particle−particle interaction dynamics can be well understood. Two differently sized polystyrene micro-particles (4.8 and 25 μm, respectively) were used in order to achieve pronounced interaction effects. The particulate was subjected to a 2-MHz ultrasonic standing wave in a microfluidic channel, such as commonly used for acoustophoresis. Observation of deflections in the particle pathways shows that the particle interaction force is not negligible under this circumstance and has to be considered in accurate particle manipulation applications. The effect is primarily pronounced when the distance between two particles is small, the sizes of the particles are different, and the acoustic properties of the particles are different relative to the media. As predicted by theory, the authors also observe that the interaction forces are affected by the angle between the inter-particle centerline and the axis of the standing wave propagation direction.
 https://doi.org/10.1121/1.5110303

[BET] Pages: 3311–3319

I. INTRODUCTION

In recent decades, a multitude of microfluidic devices utilizing acoustic forces for cell manipulation and separation in biomedical applications has been developed (Gröschl, 1998; Antfolk and Laurell, 2017). In such devices, acoustic effects originating from either primary radiation forces, secondary radiation forces, or acoustic streaming are combined in order to determine the final particle trajectories during manipulation. Among these effects, the primary acoustic radiation force and acoustic streaming (Wiklund *et al.*, 2012; Huang *et al.*, 2014) have been widely investigated and used in various devices for cell separation (Li *et al.*, 2015), cell trapping (Nilsson *et al.*, 2009; Lee *et al.*, 2013; Tenje *et al.*, 2015), bacteria trapping (Hammarström *et al.*, 2012; Hammarström *et al.*, 2014a), cell sorting (Li *et al.*, 2015), tissue culture (Li *et al.*, 2014), and cell, particle, and fluid manipulation (Dual *et al.*, 2012; Barani *et al.*, 2016).

The radiation force acting on a particle in the acoustic field is called the primary radiation force, $\boldsymbol{F}^{\mathrm{rad}}$, which was theoretically introduced by King (1934), and further developed by Yosioka and Kawasima (1955), Gorkov (1962), and Doinikov (2002). Recently, Karlsen and Bruus (2015) improved the theory by considering the effect of a thermoviscous boundary layer. They also considered the effect of acoustic streaming on the fluid flow which can influence particles or cell manipulation by Stokes drag force.

In addition to these forces, the secondary radiation force can be influential in the case where two or more particles are close to each other (Gröschl, 1998). Under this condition, particles that are exposed to the acoustic field sense secondary acoustic forces due to the scattered wave from other particles (Sepehrirahnama *et al.*, 2015) as well as the primary acoustic force. This force was theoretically investigated by Bjerknes (1906) already in 1906. He studied the acoustic interaction forces between a pair of air bubbles in stationary acoustic field and assumed that the surrounding fluid is inviscid and incompressible. This theoretical work was followed up by Crum (1975) who experimentally studied the Bjerknes forces acting on a pair of air bubbles in a stationary sound field. In 1984, Weiser *et al.* (1984) studied the mutual interaction between particles in a standing wave both theoretically and experimentally. They considered the case when the gravitational and time-averaged acoustic forces were in balance with each other and compared their theory with experimental observations. In 1995, Zheng and Apfel (1995) investigated the acoustic interaction forces between two fluid spheres in a plane acoustic wave field. They mentioned that the direction and the magnitude of the inter-particle force depends strongly on the orientation of the centerline distance between two particles, relative to the acoustic field. By considering the incompressible viscous fluid, Doinikov (2002)

[a)]Also at: Department of Applied Physics, Royal Institute of Technology, KTH-AlbaNova, SE-106 91 Stockholm, Sweden.
[b)]Electronic mail: martin.wiklund@biox.kth.se

calculated the time-averaged interaction forces between the two gas bubbles in an acoustic field. He showed that for small bubbles there is a wide parameter range that causes bubbles to repel each other, which was contrary to the classical Bjerknes theory.

More recently, several studies have addressed the effect of Bjerknes forces on bubbles experimentally and theoretically (Doinikov, 1999; Yamakoshi and Koganezawa, 2005; Yasui *et al.*, 2008; Garcia-Sabaté *et al.*, 2014). For example, Garcia-Sabaté *et al.* (2014) introduced an experimental method for measuring the inter-particle force between two solid particles. They used a 2.5 MHz nominal frequency transducer to generate standing wave in the channel. They extracted an inter-particle force on the order of 10^{-14} N for latex particles of size range 5–15 μm when particles were located in the pressure nodal line. Silva and Bruus (2014) presented a theoretical expression for inter-particle forces between small spherical particles (much smaller than the acoustic wavelength) in an ideal fluid. The method that they presented is applicable for either standing waves or traveling plane waves. Their results show that in the wave propagation direction an aggregation region appears while in the transverse direction repelling and attraction can occur. Baasch *et al.* (2017) implemented a semi-analytical method to simulate the trajectory of particles considering the interaction of particles as well as the primary forces. Habibi *et al.* (2017) also studied the effect of material properties and particle size on primary and secondary acoustic forces. In their study, they used large particle diameters up to the acoustic wavelength. In another study, Lopes *et al.* (2016) theoretically analyzed the acoustic interaction forces and torques between Mie particles having sizes comparable to the wavelength. In more recent work Mohapatra *et al.* (2018) measured the inter-particle acoustic forces in the case where two particles are in close proximity while approaching the pressure nodal plane with the center to center lined up perpendicular to the wave propagation direction. Their results show remarkable difference between the experimental results of secondary acoustic force related to the value predicted by theoretical estimation.

Due to the complexity of measurements of particle interaction forces, for example, the challenge in decoupling primary and secondary force effects, studies until now focused on solid particles in the nodal pressure line (Garcia-Sabaté *et al.*, 2014) or bubbles (Crum, 1975; Engebrecht, 2009; Pelekasis *et al.*, 2004). In the case of bubbles, they are dominated by compressibility effects of the secondary acoustic radiation force and the dipole effect is therefore negligible. In the case of studying solid particles located in the pressure nodal plane in an ideal one-dimensional standing wave, the situation is simplified since there are no primary acoustic radiation forces in this nodal plane. Instead, any measured particle motion can then be considered to originate from the secondary acoustic radiation force, given that gravity and other non-acoustic forces can be neglected. This means that for such solid particles in the pressure nodal plane, the compressibility-dependent monopole effect vanishes.

In the current study we designed a new method for characterizing the inter-particle forces between particles by considering both monopole and dipole effects of secondary acoustic radiation forces. Based on this method we observed the inter-particle forces for polystyrene particle located outside of the pressure node for the first time. Therefore, this investigation also addresses the angle dependency of the dipole effect in acoustic particle−particle interaction force.

To reach the goal of this study and investigate the inter-particle forces outside the pressure node, we chose two different polystyrene particles with sizes 4.8 and 25 μm, respectively, to achieve significant and measurable interaction forces. Particle tracking velocimetry (PTV) was used to extract the acoustic particle interaction forces and acoustic energy in the channel. This method has previously been used to measure the energy density and particle velocity by Barnkob *et al.* (2010) and Augustsson *et al.* (2011). By fixing the larger particle to a static position in the channel and observing deflection in the pathway of a moving smaller particle we showed that this force could be significant during certain conditions. To compare the experimental results with theory, the semi-quantitative model by Gröschl (1998) has been used. We have also analyzed the relative positions of particle pairs at the termination of direct particle–particle contacts, and at various positions in between a pressure node and a pressure antinode. We believe our results will be important when designing future refined acoustophoresis systems taking into account both primary and secondary acoustic radiation force effects.

II. THEORY OF THE SECONDARY ACOUSTIC RADIATION FORCE

When a particle is exposed to an acoustic standing wave it will experience a time-averaged force known as the primary acoustic force, F_{pr}, which in an ideal fluid in a one-dimensional acoustic wave can be expressed as (Gor'kov, 1962)

$$F_{pr} = 4\pi r^3 E_{ac} k\, \phi\, \sin(2ky), \tag{1}$$

$$\phi = 1 - \frac{\kappa_p}{\kappa_f} + \frac{3(\rho_p - \rho_f)}{2\rho_p + \rho_f}. \tag{2}$$

Here, E_{ac} is acoustic energy density, ϕ is acoustic contrast factor, k is wave number, and y is distance from the first pressure node. Furthermore, ρ_f is fluid density, ρ_p is the particle density, κ_p is the particle compressibility, and κ_f is the fluid compressibility. In addition to primary acoustic radiation forces, secondary acoustic radiation forces also can be influential. Such secondary forces refer to interaction forces between two bubbles or particles and can be divided in two major components relating to compressibility and density difference of the particle and the medium. The effect of compressibility is considered in the formula derived by Apfel (1988) where the secondary acoustic force, F_{se} is described as

$$F_{se} = -\frac{2\pi\rho_f}{9}(\kappa_f \omega P_a)^2 \left(1 - \frac{\kappa_{p1}}{\kappa_f}\right)\left(1 - \frac{\kappa_{p2}}{\kappa_f}\right)\left(r_{p1}^3 r_{p2}^3/d^2\right), \tag{3}$$

where P_a is the pressure amplitude and index 1 and 2 refer to the two different particles or bubbles, d is center to center distance between two objects, and ω is the angular frequency.

In the case where we have two rigid spherical particles, the inter-particle force depends on the angle of centerline and the wave propagation direction, θ, as well as difference of density of particles and medium. Based on Weiser *et al.* (1984), this force can be evaluated for two particles with the radius of r_{p1} and r_{p2} in the following forms:

$$F_0 = \frac{2\pi(\rho_p - \rho_f)^2 v_{ac}^2 r_{p1}^3 r_{p2}^3}{3\rho_f d^4},$$
$$F_{se} = F_0(3\cos^2\theta - 1), \tag{4}$$

where v_{ac} is the acoustic velocity of the incident acoustic wave at the position of the sphere. As shown in above equations, the monopole and dipole effects are considered separately. Gröschl (1998) introduced an approximate formula based on the study by Crum (1971) using superposition of forces and considering the effect of the particle position, y, in the channel:

$$F_{se}(y) = 4\pi r^6 \left\{ \frac{(\rho_p - \rho_f)^2(3\cos^2\theta - 1)}{6\rho_f d^4} v^2(y) - \frac{\omega^2 \rho(\kappa_p - \kappa_f)^2}{9d^2} p^2(y) \right\}, \tag{5}$$

where $v(y)$ and $p(y)$ are the unperturbed incident velocity and pressure fields at the particle position, respectively. The first term in this equation contains the density effect and is orientation dependent as well as particle position dependent. This term causes either attraction or repulsion depending on the lineup angle between two particles. For this first density-dependent term (the dipole term), the dependency of the interaction force on the distance decays with d^{-4}. The second compressibility-dependent term (the monopole term) is not orientation dependent and has a distance dependence decaying with d^{-2}. The monopole term is position dependent and in the pressure node of a one-dimensional standing wave it is eliminated while on the other hand, the dipole term is eliminated in the pressure antinode. However, in between the pressure node and the antinode, both term contributes to the secondary radiation force, which is the case studied in this work.

Recently, Silva and Bruus (2014) expressed a detailed formulation based on scalar potential theory with no restriction on center to center particle distances. This model is compared with the Gröschl (1998) formulation [Eq. (5)] when analyzing our experiments (cf. Sec. III).

III. MATERIALS AND METHODS

A. Experimental apparatus

The acoustofluidic device, previously described by Manneberg *et al.* (2008), consisted of a 2-MHz half-wavelength microchannel etched in silicon with the cross-section area $375 \times 110\,\mu m^2$ (width × height). Top and bottom of the channel are sealed using glass, and a lead zirconium titanate (Pz-26, Ferroperm AC, Denmark) transducer with a 2-MHz serial resonance is attached using a thermally conductive gel (Tensive Adhesive, Parker Laboratories, Fairfield, NJ).

The acoustic field was generated by actuating the transducer with a signal generator (DS345, Stanford Research Systems, CA) with a maximum output voltage of 10 V_{pp}. At this voltage, the expected temperature increase in our device is at most on the order of a few °C (Svennebring *et al.*, 2007), and the corresponding relative resonance frequency shift is of the 10^{-3} (Hammarström *et al.*, 2014b). Signal monitoring was carried out with a digital oscilloscope (TDS620B, Tektronix Inc., Beaverton, OR). In order to control the fluid flow, stop-valves were used at both the inlet and the outlet of the channel. The monitoring system of particle motion includes an optical microscope and a monochromatic camera (Point Grey, Grasshopper®3-GS3-U3-41C6M-C) connected to a computer. An overview of the experimental setup is shown in Fig. 1.

B. Fluid and particle properties

Polystyrene micro-beads with diameters 4.8 and 25 μm (Polystyrene micro-particles, KISKER) were used in the experiments. Polystyrene suspended in water was selected for this study since it has well-known material properties. These properties are listed in Table I.

C. Experimental procedure

The micro-channel was first primed by flushing deionized (DI) water. Subsequently, 25 μm polystyrene particles in pure DI water were injected, and these particles were allowed to settle for 2 h and stick to the channel bottom at arbitrary positions due to the absence of detergents. Thus, the positions of the 25 μm particles were fixed during all experiments. This was achieved by 2 h of incubation, resulting in adhesion forces between the 25 μm particles and the channel bottom dominating over all other forces acting on the particles, including the acoustic radiation forces. After this anchoring procedure of the larger particles at fixed positions in the channel, 4.8 μm particles in DI water supplemented with 0.01% Tween-20 (Sigma Aldrich, MO) were injected to the channel. The concentration of Tween-20 detergent was sufficient to prevent any fixation of the 4.8 μm particles, while the experiment time was short enough to retain all 25 μm particles at their fixed positions despite the presence of the detergent. During ultrasonic actuation, the 4.8 μm particles were driven to the pressure nodal plane in the center of the channel. However, we only analyzed the rare event where 4.8 μm particles passed nearby a fixed 25 μm particle at a distance causing a measurable deflection in the predicted particle path due to the primary radiation force, and within the same z plane close to the channel bottom [cf. Fig. 1(a)].

To enhance the effects of secondary forces in relation to the primary forces the particle sizes were carefully selected. As the secondary forces are known to scale with the volume of both particles a large size difference (25 μm versus 4.8 μm) were used in order to achieve significant secondary forces on the smaller particles. Simultaneously, the size of the small particles still needs to be large enough such that primary radiation forces dominated over acoustic streaming effects.

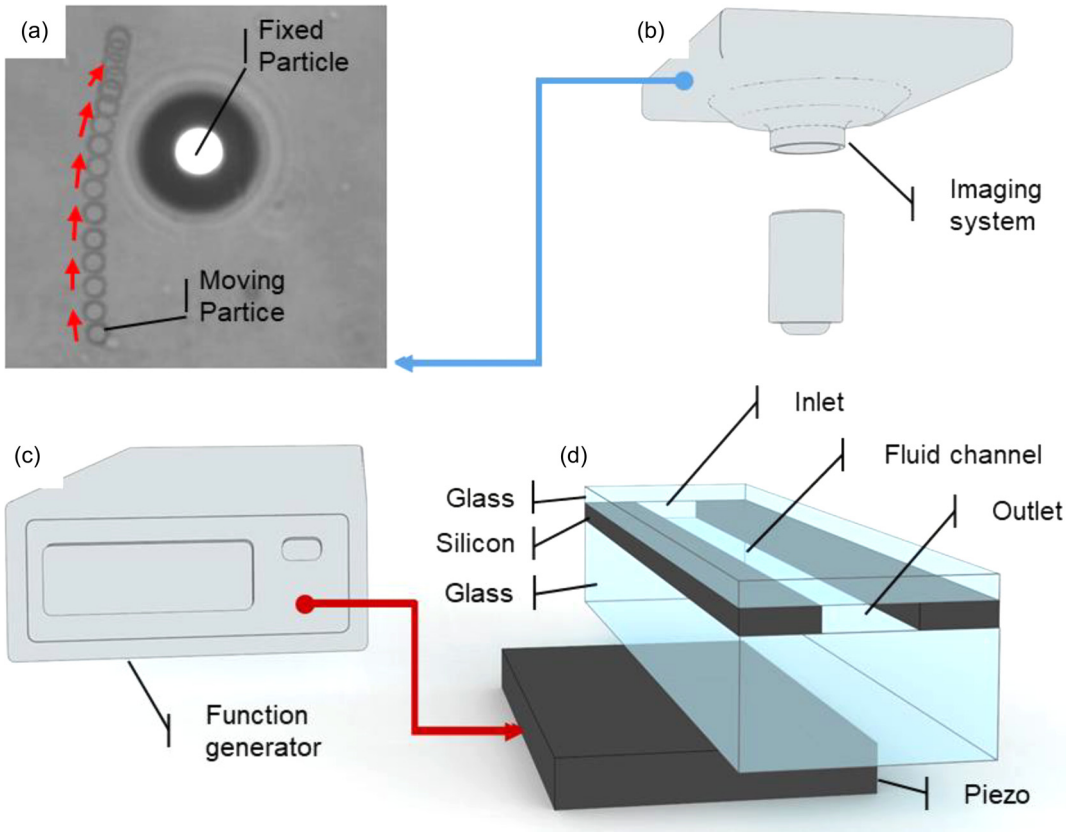

FIG. 1. (Color online) The experimental setup used to generate time-lapse images of acoustically generated motion of polystyrene small particles in close proximity of polystyrene larger stationary particles (a). The grayscale image sequences are recorded using a microscope and camera (b) starting from the onset of acoustic actuation from a signal generator (c). The microfluidic device consisted of a conventional glass-silicon-glass structure (d), equipped with stop valves and designed to produce an ultrasonic standing wave with a single pressure node in the center of the channel and aligned parallel with the channel direction at frequencies close to 2 MHz.

Once events where smaller and larger particles located in close proximity were identified, a sinusoidal signal with frequency of 2-MHz was activated and videos of particle trajectories were recorded. The particle movement was captured in 13 frame per second (fps) and in the gray-scale mode.

Before investigating acoustic inter-particle forces, we first measured the acoustic energy density in the channel by the use of the PTV method. Then, various observed events of particle−particle interaction dynamics (with and without direct contact) were considered in order to compare the experimental results with theory. For the measurements of particle interaction without any direct particle–particle contact, we studied the cases where the distance between two particles was sufficient to deflect the trajectory of the 4.8 μm particle while passing by the fixed 25 μm particle. We also studied events where the small 4.8 μm particle got in contact with the 25 μm particle. For these events, we analyzed the particle positions when the contact was terminated by measuring the separation angle between the particle–particle centerline and the sound field gradient.

TABLE I. Acoustic properties of the fluid and micro-particles.

	Density (kg/m^3)	Speed of sound (m/s)
Water	998	1480
Polystyrene	1056	2400

IV. RESULT AND DISCUSSION

A. Inter-particle force estimation

In order to analyze the data, the velocity of moving particles in x and y directions were extracted separately. By considering the Stokes drag, $F_{\text{drag}} = 6\pi\eta v r_{\text{p}}$, in laminar flow the net force in x and y direction was evaluated. In this formula, η is dynamic viscosity, v relative velocity of particle and surrounded medium, and r_{p} is particle radius. Since the velocity of the particle can be measured in each video frame, F_{drag} can be calculated. This force was considered as the force balancing all acoustic forces acting on a particle, although other forces may contribute to the total force as discussed in Sec. IV C below. The force in perpendicular direction to the wave propagation was considered to be purely an inter-particle acoustic force in this direction. This assumption is based on considering the standing wave field as a purely one-dimensional field, which was also confirmed from the energy density measurements. The force component was compared with the theory [cf. Eq. (5)]. Effect of compressibility and density on particle interaction force were evaluated by implementing the Gröschl model. In the case that contact occurred between two particles the data in the contact region has been eliminated. All captured videos were analyzed using Tracker, an open source particle tracing software (Brown, 2017).

B. Estimating acoustic energy in the channel from single-particle tracks

The energy density in the channel was obtained by the use of Stokes drag force and the Gor'kov equation [Eqs. (1) and (2)] for one-dimensional acoustic fields, and combined with the PTV method by tracking the paths of 4.8 μm polystyrene particles from three independent experiments. The normalized velocities of particles are depicted in Fig. 2 and compared with the velocity obtained by the Stokes and the Gor'kov's equation with the same level of energy. By using this method, the energy density of the channel was found to be 3.5–7 J/m^3 at the utilized actuation voltage 10 V_{pp}, and we also confirmed that there was no significant particle motion in the direction of the channel axis during this calibration procedure.

C. Non-acoustic force effects

It is of interest to discuss other forces that may affect the particles while they are passing by each other at close distance. Such possible forces that may influence the trajectory of the smaller particles are related to hydrodynamic interactions, van der Waals interaction and lubrication forces.

1. Hydrodynamic interaction

Based on the study of Mohapatra *et al.* (2018), the effect of hydrodynamic interaction between two particles could be consider by using the following equation:

$$\begin{Bmatrix} U_1 \\ U_2 \end{Bmatrix} = \frac{1}{6\pi\mu a}\begin{pmatrix} 1 & C \\ C & 1 \end{pmatrix} \times \begin{Bmatrix} F_1 \\ F_2 \end{Bmatrix}, \tag{6}$$

where U, C, and F are velocity, a dimensionless parameter dependent on particle size and position, and force acting on each particle, respectively. Index 1 and 2 also refer to first and second particle. In our case the larger particle is fixed, which means that there is no motion of this particle relative the fluid medium. Using Eq. (6), we may calculate the magnitude of the hydrodynamic interaction effect relative the drag force from the simple Stokes theory. For the particle−particle distances observed in our experiments, the average absolute deviation from Stokes theory is 16% when comparing Stokes theory with hydrodynamic interaction, with a maximum deviation of 49%. This needs to be taken into account when comparing experimental results with the theory.

Furthermore, when a particle gets close to a wall the drag force acting on the particle increases with a coefficient related to the particle−wall distance and the direction of particle motion relative the wall. Brenner (1961) as well as Happel and Brenner (1983) defined formulas to calculate this force for different particle−wall distances and for the Reynolds number larger than 0.1. Even at low Reynolds number (in our case in the range of 10^{-5}) the effect may be significant, in particular when particles are translated close to a wall (Leach *et al.*, 2009). In our case, the analyzed particles are always close to the channel bottom, which may contribute to a non-negligible but constant additional drag force.

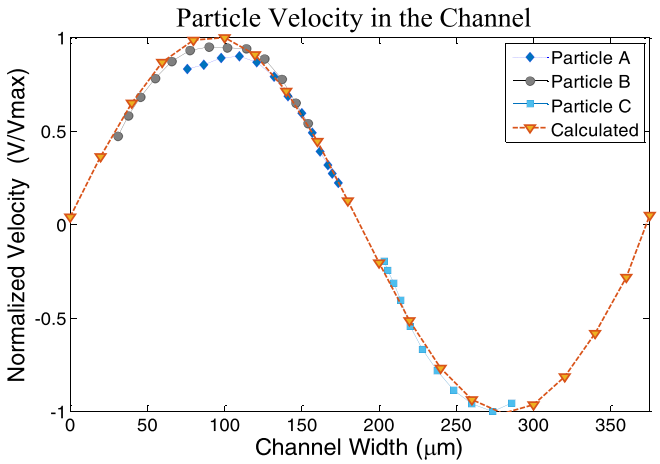

FIG. 2. (Color online) Profile of normalized velocity from three different measurements in order to evaluate the energy density of the channel due to the standing acoustic field (4.8 μm polystyrene particles).

2. Van der Waals force

Over small, nanometer range, distances between two particles the van der Waals force may play an important role. The van der Waals force in the proximity of two close spherical particles can be estimated by the following formula (Israelachvili, 2011):

$$F_{\mathrm{Van}} = -\frac{Ar_1r_2}{6h_0^2(r_1+r_2)}, \tag{7}$$

where A is the Hamaker constant which is 6.6–7.9 $\times 10^{-20}$ J for polystyrene, h_0 is the distance between the particle surfaces, and r_1 and r_2 are the two particle radii. In our experiments we cannot measure distances on the nanometer scale. Nonetheless, we believe van der Waals forces may be significant in the case where we measure the particle positions at terminated particle–particle contacts (cf. Sec. IV F).

3. Lubrication force

In the case where two particles get close to each other, due to the fluid in between the particles, the lubrication force can be important. This force depends on the distance between the two particles as well as their relative velocity. For two rigid particles this force can be estimated by following formula (Barnocky and Davis, 1989; Davis *et al.*, 1989):

$$F_{\mathrm{Lub}} = 6\pi\mu r^2 W/h_0, \tag{8}$$

where W is the relative velocity between two particles and μ is the dynamic viscosity. This force acts on the particles both at close distances, and at direct contact. The lubrication force is effective at surface distances (Vázquez-Quesada and Ellero, 2016; Lambert *et al.*, 2018) of $0 < h_0 < \epsilon r$ where $0 < \epsilon \ll 1$. It means that, in our case, the lubrication force is relevant over nanometer distances which cannot be measured accurately in our experiment.

D. Lateral movement of particle due to existence of inter-particle force

To investigate the lateral movement of particles undergoing acoustophoresis due to inter-particle forces, we

analyzed events where a 4.8 μm particle is driven towards the pressure node while at the same time passing by a fixed 25 μm particle located somewhere in between the pressure antinode and pressure node. Here, lateral movement is defined relative the pressure gradient in the standing wave field, i.e., in the direction parallel with the channel and perpendicular to the pressure gradient. Under this condition the trajectory in the x-y plane of small particles are observed. In Fig. 3 a fixed 25 μm particle and the trajectory of small particles are shown in three different fixed particle positions and for eight different particle paths. It is clear that the small particle's path was deflected laterally (along x) by the presence of the fixed larger particle even though the moving and fixed particles are physically separated during the whole path. The small moving particles were attracted towards the larger fixed particle from both sides, Fig. 3(b). The centerline distance between the two particles influences the deflection in such a way that when this distance decreases, larger deflection in the pathway occurs. Qualitatively, the observed behavior agrees well with the secondary force interaction predicted by theory [Eq. (5)]. In addition, particles with similar starting positions repeatedly show the same behavior in the pathway deflection.

In the following two experiments, by considering the minimum contact or no contact between moving and fixed particles we studied further details of inter-particle forces and compared with theory. Here, degree refers to the angle θ between the line connecting the centers of the two particles and the wave propagation direction (the latter being equal to the direction of the pressure gradient in the one-dimensional standing wave).

As seen in Fig. 4, significant particle attraction due to inter-particle forces is observed in both cases (a,b and c,d, respectively) when the angle θ is close to 90°. As shown, the pathway of small moving particles is almost constant before and after the vicinity of the fixed particle. Comparison between experimental and theoretical results of inter-particle forces is shown in Figs. 4(b) and 4(d). Here, we compared with both the Gröschl (1998) model, as well as with the Silva and Bruus (2014) model. In the graphs negative and positive y coordinates indicate the positions of small moving particles before and after reaching the fixed particle, respectively. Here, the origin of the coordinate system is set to the center of the fixed particle. As seen in Fig. 4, although the behavior of interaction force from experimental data is in agreement with theory, there are important differences as well. In the first case [Figs. 4(a) and 4(b)], where the minimum particle–particle distance is very small, we notice a significant difference in the magnitude of the secondary acoustic force compared to what is predicted by the theory. We also notice a significant difference between the two theoretical models. It confirms that theory does not include all the possible effective parameters on secondary acoustic force at very close particle–particle distances, as discussed in the Sec. IV C. Similar results were obtained by Mohapatra *et al.* (2018) who reported a difference between theory and experimental data of similar magnitude. In the second case, however [Figs. 4(c) and 4(d)], where the minimum particle–particle distance is relatively larger compared to the first case, we notice a better agreement between experimental and theoretical data, as well as between the two theoretical models. RMSE values for these two cases are 29.5 fN and 11.7 fN, respectively. Effects of acoustic primary and secondary forces on separation position are studied further in Sec. IV F.

E. Particle pathway deflection due to acoustic force ratio

To compare the magnitude of the secondary radiation force relative the primary radiation force as a function of particle–particle distance, we analyzed these two forces under decoupled conditions. This situation is obtained when the forces are orthogonal, i.e., when the secondary radiation

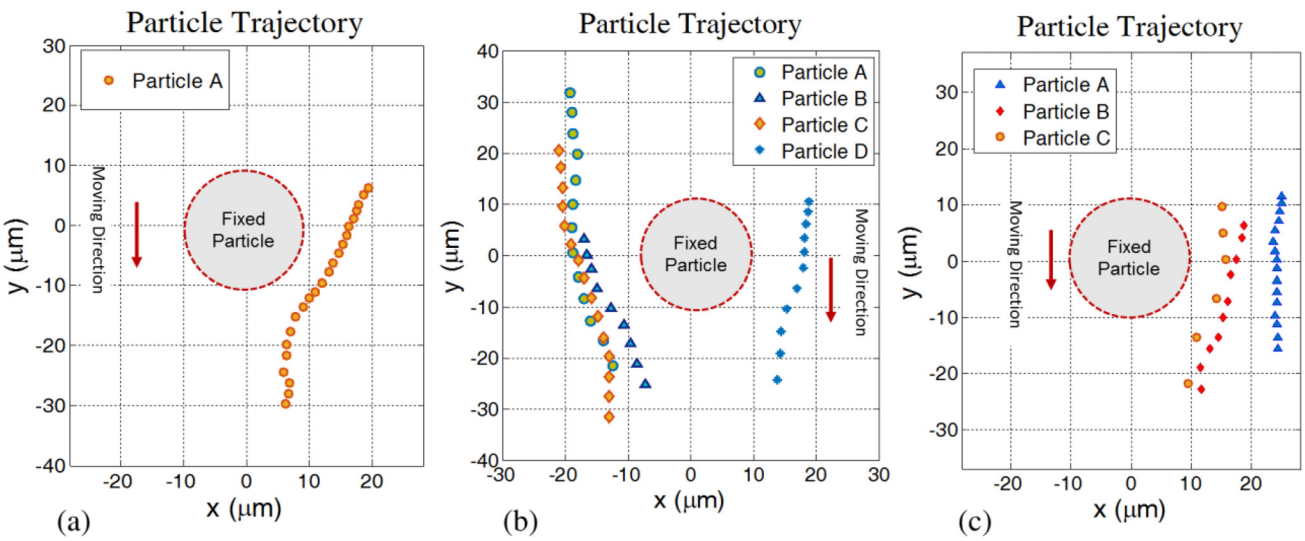

FIG. 3. (Color online) Pathway deflection of small particles due to a combination of primary and secondary acoustic radiation forces in three different cases, a, b, and c, and for in total eight different particle paths. In each case the big (25 μm) particle is fixed and small (4.8 μm) particle initially located in close proximity to the fixed particle. In b and c, in each experiment just one small particle was located in proximity of fixed particle but graph shows them all in the same time for better comparison.

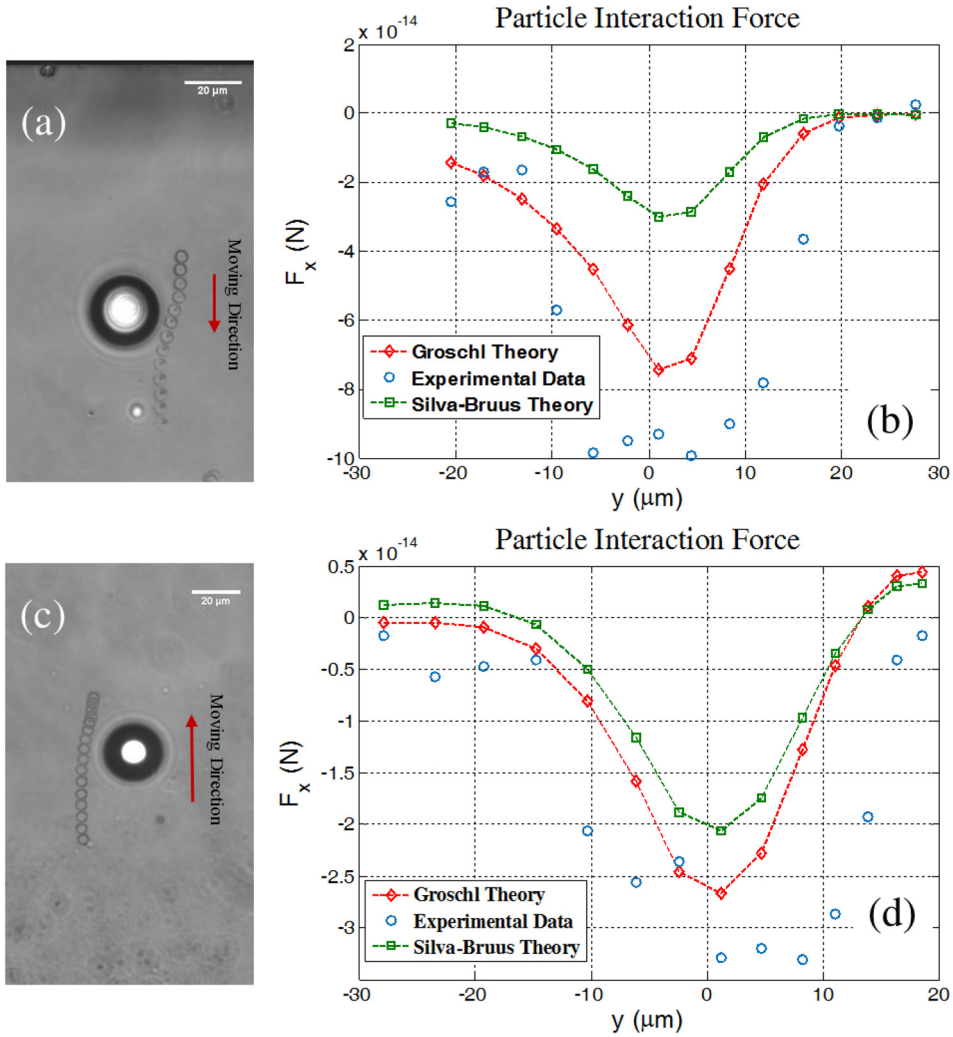

FIG. 4. (Color online) Analysis of the lateral force component of the secondary acoustic radiation force, based on (a),(c): the trajectory of moving 4.8 μm particles exposed to a standing acoustic field and passing by a fixed 25 μm particle; and (b), (d): comparison between the lateral component of the particle interaction forces measured experimentally and theoretically based on Gröschl (1998) theory, and Silva and Bruus (2014) theory. Note that a negative secondary acoustic radiation force is an attractive force.

force only has an x-component (along the channel) and the primary radiation force only has a y-component (across the channel). Figure 5 shows this ratio F_x/F_y calculated from five different experiments when the moving and fixed particles are lined up in perpendicular direction relative to the wave propagation (or pressure gradient) direction, e.g., θ is equal to 90 ± 7 deg. This angle is important for being able to decouple the primary and secondary acoustic radiation forces. Furthermore, to eliminate the position dependency of Gröschl theory [cf. Eq. (5)], fixed particles with almost the same position, less than $0.05 \times \lambda/2$ difference in particles' center position in the wave propagation direction, close to the pressure antinode is chosen. In these cases, it is expected that the role of the dipole effect will be strongly reduced, and the compressibility term will dominate in the inter-particle force. The reason is primarily that close to the pressure antinode, the acoustic velocity has small magnitude and consequently also the dipole term in Eq. (5) is less effective. In Fig. 5, the fitted power curve shows that the relation of the force ratio with center to center distances is almost equal to power of -2 which is in agreement with the compressibility part of Gröschl theory. Here, we recall that inter-particle forces in Gröschl theory are related to distance to the power -4 for the dipole effect and to the distance to the power of -2 for the monopole effect [cf. Eq. (5)]. It is also notable that the secondary radiation force can reach magnitudes on the order of 10%–20% of the primary force at typical distances around 20 μm for our settings. This means that the secondary radiation force should be taken into account in many

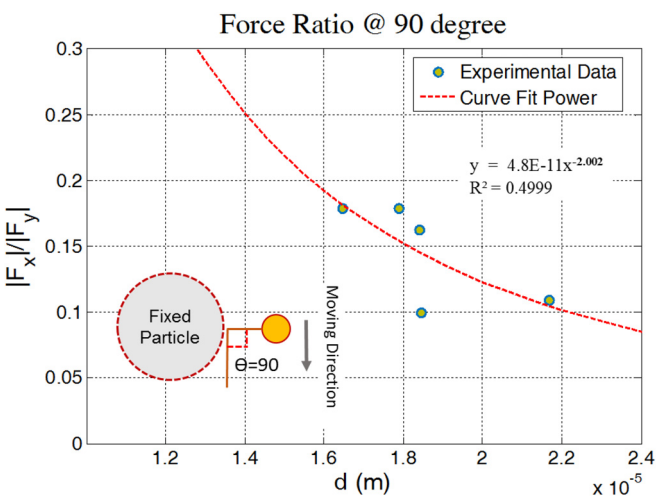

FIG. 5. (Color online) Force ratio between the secondary and primary acoustic radiation forces as a function of center-to-center particle–particle distance when lined up at the angle $90 \pm 7°$ (perpendicular to the propagation direction of the wave).

of today's acoustophoresis applications where the particle concentration most often is relatively high.

However, different inter-particle distances were also considered in Fig. 3(c). For example, there is no significant impact from secondary radiation forces on the particle path for "Particle A" in Fig. 3(c). This particle has a distance more than five times diameter of the small particle during its whole path. This means that even if the secondary radiation force has a predicted magnitude on the order of 10%–20% of the primary force, this force only acts during a very limited time and position compared to the primary acoustic radiation force. However, for larger particle concentrations, the secondary radiation force should be taken into account for accurate acoustophoresis modelling.

F. Inter-particle forces at direct particle–particle contact

Another aspect of the effect of primary and secondary acoustic radiation forces on the behavior of particles while they are in contact with each other is related to the separation angle and corresponding force ratio, see Fig. 6. Here, the separation angle is defined between the particle–particle centerline and the pressure gradient direction, when the particle–particle contact is terminated (cf. Fig. 6). To find this angle, the distance between two particles was considered. When particles get in contact with each other, the particle–particle distance is almost constant (corresponding to the sum of their radii). At a certain separation position where the particle–particle contact is terminated, the distance between particles suddenly increases. In Fig. 6, we measured the force acting on x direction (perpendicular to wave propagation direction) to force in y direction ratio as a function of the corresponding angle between particles (relative the pressure gradient) at the separation position. Here, the force ratio depends primarily on the y coordinate of the fixed particle, i.e., the position of the fixed particle relative the pressure node. Results show that by decreasing this force ratio (F_x/F_y), the moving particle separates earlier compared to the case when the force ratio is considerably higher, which corresponds to two particles being in contact with each other during a longer time. Furthermore, we also note one interesting case in Fig. 6 where the force ratio is larger than 1. This means that the secondary acoustic force is larger than the primary force, which is the case for particle pairs located close to the pressure nodal line where the primary force vanishes. This result is also important in, e.g., acoustophoretic separation processes, where particles get close to each other and often have contacts. This may lead to increasing or decreasing purity of the separation.

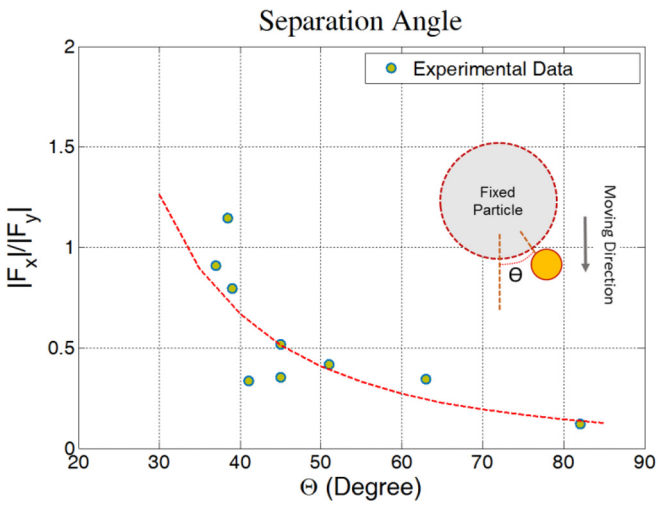

FIG. 6. (Color online) Force ratio between the secondary and primary acoustic radiation forces as a function of the angle between the particle centerline and the propagation direction of the wave, at the position where the particles are released from each other after a period of direct contact.

V. CONCLUSION

We have investigated a new method that was introduced to measure the inter-particle secondary acoustic radiation forces outside of the pressure node in a standing wave acoustophoresis micro-channel. Our results show that the inter-particle forces can play an important role in acoustophoretic particle manipulation applications and cause deflection in the particle pathway, especially in the case where the size difference between the particles is significant and particles are close to each other. The results also show that when two particles are in contact with each other, the ratio of the inter-particle forces to the primary forces can cause either rapid separation or postpone the separation when the force ratio is low and high, respectively. This can be beneficial if taken into account when designing acoustophoresis devices intended for high particle concentrations. The inter-particle forces can cause particles to make contact with each other over small distances and therefore affect the separation purity. Results also show that for inter-particle distances about five times of the diameter of a moving particle, the pathway deflection is negligible for polystyrene beads, even when interacting with a fixed particle of diameter five times larger. The presented method also provides a way to measure and decouple the monopole and dipole effects of inter-particle forces. Still, there is a significant difference in magnitude between experimental data and theoretical models. This needs to be taken into account in future studies aiming for higher quantitative precision, for example by including detailed modelling of non-acoustic force contributions. Nonetheless, the current study is to our knowledge the first experimental measurement of inter-particle acoustic radiation forces between elastic particles outside of the pressure node in a standing wave with arbitrary particle pair orientations relative the pressure gradient.

ACKNOWLEDGMENTS

We thank the Ministry of Science, Research and Technology of Iran, and the Swedish Research Council for financial support of this study.

Antfolk, M., and Laurell, T. (**2017**). "Continuous flow microfluidic separation and processing of rare cells and bioparticles found in blood—A review," Anal. Chim. Acta **965**, 9–35.

Apfel, R. E. (**1988**). "Acoustically induced square law forces and some speculations about gravitation," Am. J. Phys. **56**, 726–729.

Augustsson, P., Barnkob, R., Wereley, S. T., Bruus, H., and Laurell, T. (**2011**). "Automated and temperature-controlled micro-PIV measurements

enabling long-term-stable microchannel acoustophoresis characterization," Lab Chip **11**, 4152–4164.
Baasch, T., Leibacher, I., and Dual, J. (**2017**). "Multibody dynamics in acoustophoresis," J. Acoust. Soc. Am. **141**, 1664–1674.
Barani, A., Paktinat, H., Janmaleki, M., Mohammadi, A., Mosaddegh, P., Fadaei-Tehrani, A., and Sanati-Nezhad, A. (**2016**). "Microfluidic integrated acoustic waving for manipulation of cells and molecules," Biosens. Bioelectron. **85**, 714–725.
Barnkob, R., Augustsson, P., Laurell, T., and Bruus, H. (**2010**). "Measuring the local pressure amplitude in microchannel acoustophoresis," Lab Chip **10**, 563–570.
Barnocky, G., and Davis, R. H. (**1989**). "The lubrication force between spherical drops, bubbles and rigid particles in a viscous fluid," Int. J. Multiph. Flow. **15**, 627–638.
Bjerknes, V. F. K. (**1906**). *Fields of Force* (Columbia University Press, New York).
Brenner, H. (**1961**). "The slow motion of a sphere through a viscous a plane surface," Chem. Eng. Sci. **16**, 242–251.
Brown, D. (**2017**). "Tracker 4.11.0: Free video analysis and modeling tool for physics education," https://physlets.org/tracker/index.html (Last viewed May 7, 2018).
Crum, L. A. (**1971**). "Acoustic force on a liquid droplet in an acoustic stationary wave," J. Acoust. Soc. Am. **50**, 157–163.
Crum, L. A. (**1975**). "Bjerknes forces on bubbles in a stationary sound field," J. Acoust. Soc. Am. **57**, 1363–1370.
Davis, R. H., Schonberg, J. A., and Rallison, J. M. (**1989**). "The lubrication force between two viscous drops," Phys. Fluids A **1**, 77–81.
Doinikov, A. A. (**1999**). "Bjerknes forces between two bubbles in a viscous fluid," J. Acoust. Soc. Am. **106**, 3305–3312.
Doinikov, A. A. (**2002**). "Viscous effects on the interaction force between two small gas bubbles in a weak acoustic field," J. Acoust. Soc. Am. **111**, 1602–1609.
Dual, J., Möller, D., Neild, A., Oberti, S., Schwarz, T., and Wang, J. (**2012**). "Particle manipulation using acoustic radiation forces in micromachined devices," AIP Conf. Proc. **1433**, 27–32.
Engebrecht, C. P. (**2009**). "Bubble dynamics in ultrasound," M.Sc. thesis, University of Washington.
Garcia-Sabaté, A., Castro, A., Hoyos, M., and González-Cinca, R. (**2014**). "Experimental study on inter-particle acoustic forces," J. Acoust. Soc. Am. **135**, 1056–1063.
Gor'kov, L. P. (**1962**). "On the forces acting on a small particle in an acoustical field in an ideal fluid," Sov. Phys. Dokl. **6**, 773–775.
Gröschl, M. (**1998**). "Ultrasonic separation of suspended particles—Part I: Fundamentals," Acustica **84**, 432–447.
Habibi, R., Devendran, C., and Neild, A. (**2017**). "Trapping and patterning of large particles and cells in a 1D ultrasonic standing wave," Lab Chip **17**, 3279–3290.
Hammarström, B., Evander, M., Wahlström, J., and Nilsson, J. (**2014b**). "Frequency tracking in acoustic trapping and system surveillance," Lab Chip **14**, 1005–1013.
Hammarström, B., Laurell, T., and Nilsson, J. (**2012**). "Seed particle-enabled acoustic trapping of bacteria and nanoparticles in continuous flow systems," Lab Chip **12**, 4296–4304.
Hammarström, B., Nilson, B., Laurell, T., Nilsson, J., and Ekström, S. (**2014a**). "Acoustic trapping for bacteria identification in positive blood cultures with MALDI-TOF MS," Anal. Chem. **86**, 10560–10567.
Happel, J., and Brenner, H. (**1983**). *Low Reynolds Number Hydrodynamics: With Special Applications to Particulate Media* (Springer Netherlands, The Hague).
Huang, P., Nama, N., Mao, Z., Li, P., Rufo, J., Chen, Y., Xie, Y., Wei, C. H., Wang, L., and Huang, T. J. (**2014**). "A reliable and programmable acoustofluidic pump powered by oscillating sharp-edge structures," Lab Chip **14**, 4319–4323.
Israelachvili, J. N. (**2011**). *Intermolecular and Surface Forces* (Academic, New York).
Karlsen, J. T., and Bruus, H. (**2015**). "Forces acting on a small particle in an acoustical field in a thermoviscous fluid," Phys. Rev. E **92**, 043010.
King, L. V. (**1934**). "On the acoustic radiation pressure on spheres," Proc. R. Soc. London Ser. A **147**, 212–240.
Lambert, B., Weynans, L., and Bergmann, M. (**2018**). "Local lubrication model for spherical particles within incompressible Navier-Stokes flows," Phys Rev E **97**, 033313.
Leach, J., Mushfique, H., Keen, S., Di Leonardo, R., Ruocco, G., Cooper, J. M., and Padgett, M. J. (**2009**). "Comparison of Faxén's correction for a microsphere translating or rotating near a surface," Phys. Rev. E **79**, 026301.
Lee, J., Jeong, J. S., and Shung, K. K. (**2013**). "Microfluidic acoustic trapping force and stiffness measurement using viscous drag effect," Ultrasonics **53**, 249–254.
Li, P., Mao, Z., Peng, Z., Zhou, L., Chen, Y., Huang, P. H., Truica, C. I., Drabick, J. J., El-Deiry, W. S., and Dao, M. (**2015**). "Acoustic separation of circulating tumor cells," Proc. Natl. Acad. Sci. **112**, 4970–4975.
Li, S., Glynne-Jones, P., Andriotis, O. G., Ching, K. Y., Jonnalagadda, U. S., Oreffo, R. O. C., Hill, M., and Tare, R. S. (**2014**). "Application of an acoustofluidic perfusion bioreactor for cartilage tissue engineering," Lab Chip **14**, 4475–4485.
Lopes, J. H., Azarpeyvand, M., and Silva, G. T. (**2016**). "Acoustic interaction forces and torques acting on suspended spheres in an ideal fluid," IEEE Trans. Ultrason. Ferroelectr. Freq. Control **63**, 186–197.
Manneberg, O., Svennebring, J., Hertz, H. M., and Wiklund, M. (**2008**). "Wedge transducer design for two-dimensional ultrasonic manipulation in a microfluidic chip," J. Micromech. Microeng. **18**, 095025.
Mohapatra, A. R., Sepehrirahnama, S., and Lim, K. (**2018**). "Experimental measurement of interparticle acoustic radiation force in the Rayleigh limit," Phys. Rev. E **97**, 053105.
Nilsson, J., Evander, M., Hammarström, B., and Laurell, T. (**2009**). "Review of cell and particle trapping in microfluidic systems," Anal. Chim. Acta **649**, 141–157.
Pelekasis, N. A., Gaki, A., Doinikov, A., and Tsamopoulos, J. A. (**2004**). "Secondary Bjerknes forces between two bubbles and the phenomenon of acoustic streamers," J. Fluid. Mech. **500**, 313–347.
Sepehrirahnama, S., Lim, K. M., and Chau, F. S. (**2015**). "Numerical study of interparticle radiation force acting on rigid spheres in a standing wave," J. Acoust. Soc. Am. **137**, 2614–2622.
Silva, G. T., and Bruus, H. (**2014**). "Acoustic interaction forces between small particles in an ideal fluid," Phys. Rev. E. **90**, 063007.
Svennebring, J., Manneberg, O., and Wiklund, M. (**2007**)."Temperature regulation during ultrasonic manipulation for long-term cell handling in a microfluidic chip," J. Micromech. Microeng. **17**, 2469–2474.
Tenje, M., Xia, H., Evander, M., Hammarström, B., Tojo, A., Belák, S., Laurell, T., and LeBlanc, N. (**2015**). "Acoustic trapping as a generic non-contact incubation site for multiplex bead-based assays," Anal. Chim. Acta **853**, 682–688.
Vázquez-Quesada, A., and Ellero, M. (**2016**). "Analytical solution for the lubrication force between two spheres in a bi-viscous fluid," Phys. Fluids **28**, 073101.
Weiser, M. A. H., Apfel, R. E., and Neppiras, E. A. (**1984**). "Interparticle forces on red cells in a standing wave field," Acta Acust. united Acust. **56**, 114–119.
Wiklund, M., Green, R., and Ohlin, M. (**2012**). "Acoustofluidics 14: Applications of acoustic streaming in microfluidic devices," Lab Chip **12**, 2438–2451.
Yamakoshi,Y., and Koganezawa, M. (**2005**). "Bubble manipulation by self organization of bubbles inside ultrasonic wave," Jpn. J. Appl. Phys. **44**, 4583–4587.
Yasui, K., Iida, Y., Tuziuti, T., Kozuka, T., and Towata, A. (**2008**). "Strongly interacting bubbles under an ultrasonic horn," Phys. Rev. E **77**, 016609.
Yosioka, K., and Kawasima, Y. (**1955**). "Acoustic radiation pressure on a compressible sphere," Acustica **5**, 167–173.
Zheng, X., and Apfel, R. E. (**1995**). "Acoustic interaction forces between two fluid spheres in an acoustic field," J. Acoust. Soc. Am. **97**, 2218–2226.